DOI: 10.1002/ejic.200600661

Phase Formation and Properties in the System Bi_2O_3:$2CoO_{1+x}$:Nb_2O_5

Terrell A. Vanderah,[a] Theo Siegrist,[b] Michael W. Lufaso,*[a][‡] Margaret C. Yeager,[a] Robert S. Roth,[a] Juan C. Nino,[c] and Samantha Yates[c]

Keywords: Pyrochlore / Displacive disorder / Bismuth cobalt niobates / Bi–Co–Nb–O / Phase equilibria / Phase diagram / Dielectric properties / Magnetic properties

Subsolidus phase relations have been determined for the Bi–Co–Nb–O system in air (750–925 °C). Ternary compound formation was limited to pyrochlore ($A_2B_2O_6O'$), which formed a substantial solid solution region at Bi-deficient stoichiometries (relative to $Bi_2Co_{2/3}Nb_{4/3}O_7$) suggesting that about 8 to 25 % of the A sites are occupied by Co. X-ray powder diffraction data confirmed that all Bi–Co–Nb–O pyrochlores exhibit displacive behavior. A structural refinement of the pyrochlore $Bi_{1.56}Co_{0.96}Nb_{1.48}O_7$ using single-crystal X-ray diffraction data is reported with the A and O′ atoms displaced (0.34 Å and 0.45 Å, respectively) from ideal positions to 96g sites and 32e sites, respectively [$Fd\bar{3}m$ (#227), a = 10.551(1) Å]. The displacive structural behavior is similar to that found in analogous Bi–M–Nb–O pyrochlores (M = Zn, Fe, Mn). Bi–Co–Nb–O pyrochlores exhibited overall paramagnetic behavior with negative Curie–Weiss temperature intercepts indicating weak antiferromagnetic interactions. At 250 K and 1 MHz the relative dielectric permittivity of the pyrochlore 0.4400:0.2100:0.3500 Bi_2O_3:$2CoO_{1+x}$:Nb_2O_5 was ca. 115 with tan δ = 0.06; however, at lower frequencies the sample was conductive. Low-temperature dielectric relaxation such as that observed for $Bi_{1.5}Zn_{0.92}Nb_{1.5}O_{6.92}$ and other bismuth-based pyrochlores was not observed. Consideration of bond lengths, effective magnetic moments, and dielectric properties suggests that the average oxidation state of Co in the pyrochlore phases is close to but slightly higher than 2.0.

Introduction

Multiferroic ceramics which exhibit magnetoelectric effects display coupling between cooperative phenomena such as ferroelectricity and ferromagnetism, and have attracted considerable attention owing to their scientific and practical interest.[1] The possibility of manipulating the magnetic or dielectric properties of a single material by an applied electric or magnetic field, respectively, opens up entirely new device applications in microelectronics and data storage.[2–4] Only a few compounds are known to exhibit these properties,[3,5,6] including several Fe-[3,7] and Mn-containing[8–12] complex oxides. Currently, however, single-phase materials with magnetoelectric responses sufficiently robust for practical exploitation are not known. The present study of the Bi_2O_3–$2CoO_{1+x}$–Nb_2O_5 system was undertaken to characterize the formation and properties of ternary compounds that form from strongly polarizable (Bi_2O_3, Nb_2O_5) and magnetic (CoO_{1+x}) components.

[a] National Institute of Standards and Technology, Materials Science & Engineering Laboratory,
Gaithersburg, MD 20899, USA
[b] Bell Laboratories, Lucent Technologies,
Murray Hill, NJ 07974, USA
[c] University of Florida, Department of Materials Science & Engineering,
Gainesville, FL 32611-6400, USA
[‡] University of North Florida, Department of Chemistry & Physics,
Jacksonville, FL 32224, USA

Results and Discussion

Phase Formation

The results of the phase-equilibrium study are presented in Figure 1. In the Co–Nb–O subsystem the Co^{2+} compounds $CoNb_2O_6$ and $Co_4Nb_2O_9$ were observed.[13] The CoO:Nb_2O_5 intergrowth phases reported to form at molar ratios of 1:7, 1:18, and 1:34, respectively,[13,14] were difficult to equilibrate and exhibited highly complex X-ray powder diffraction patterns related to that of Nb_2O_5 (as expected); this region of the phase diagram is depicted to obey the phase rule but was not investigated in detail. Phase-equilibria information for the Bi_2O_3–CoO_{1+x} system has not, to the best of our knowledge, been reported. In the present study only a single phase of the sillenite-type was observed to form at $Bi_{25}CoO_{40-\delta}$.[15,16] Specimens equilibrated at 0.500:0.500 and 0.333:0.667 Bi_2O_3:$2CoO_{1+x}$ (800 °C) were mixtures of the sillenite phase and Co_3O_4 – the former composition formed considerable liquid at 850 °C, the latter at 900 °C. Giant electric polarization has been predicted for $BiCoO_3$ using first-principles methods;[17] however, the synthesis of this phase has not, to the best of our knowledge, been reported. The binary Bi–Nb–O phases observed were in general agreement with the comprehensive study reported by Roth[18] except for the high-Bi_2O_3 (≥0.75 mol fraction) region, represented in Figure 1 as a "fluorite" solid solution extending from 75:25 Bi_2O_3:Nb_2O_5 ($Bi_3Nb_2O_7$)

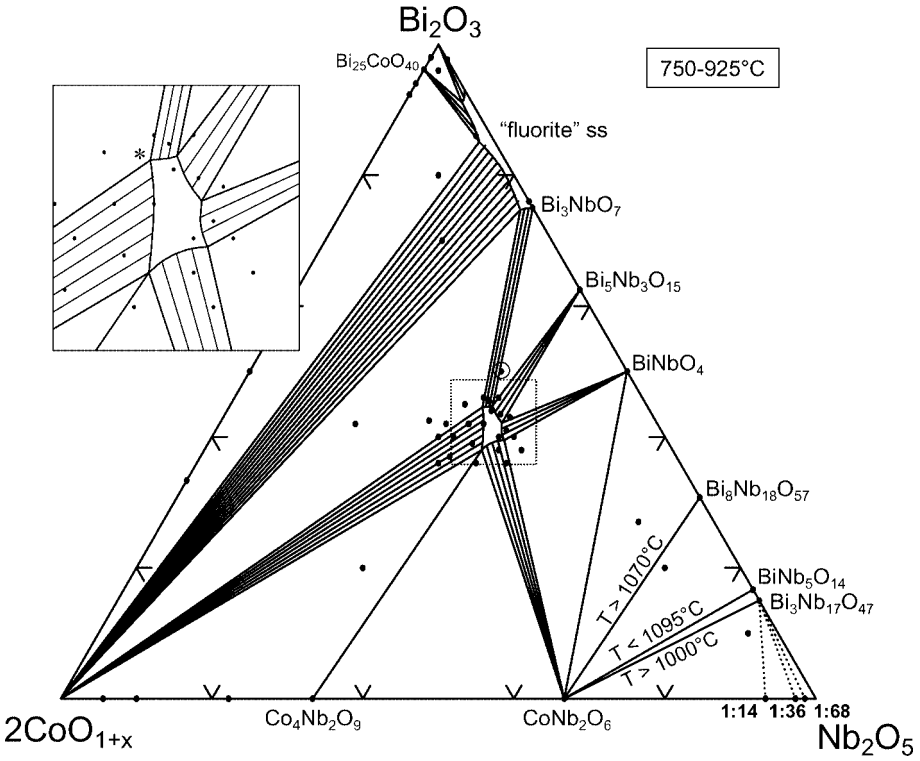

Figure 1. Subsolidus phase equilibrium diagram in air for the Bi_2O_3:$2CoO_{1+x}$:Nb_2O_5 system. Black dots denote the compositions of specimens prepared in the study; concentrations are on a molar fraction basis. Ternary phase formation is limited to pyrochlore, which forms an appreciable solid solution near the center of the diagram (enlarged in the inset). The "pyrochlore-like" composition $Bi_2Co_{2/3}Nb_{4/3}O_7$ (open circle) is not included in the solid solution region, but rather forms a three-phase mixture of Bi_3NbO_7, pyrochlore, and $Bi_5Nb_3O_{15}$. The limiting compositions of the pyrochlore field suggested by the present data are (inset: clockwise beginning with the cusp marked with an asterisk) Bi_2O_3:$2CoO_{1+x}$:Nb_2O_5 = 0.446:0.220:0.334 [$Bi_{1.79}Co_{0.88}Nb_{1.34}O_7$, a = 10.580(1) Å], 0.448:0.205:0.347 [$Bi_{1.78}Co_{0.81}Nb_{1.38}O_7$, a = 10.589(1) Å], 0.422:0.205:0.373 [$Bi_{1.65}Co_{0.80}Nb_{1.46}O_7$, a = 10.571(1) Å], 0.395:0.215:0.390 [$Bi_{1.53}Co_{0.83}Nb_{1.51}O_7$, a = 10.556(1) Å], and 0.380:0.253:0.367 [$Bi_{1.51}Co_{1.00}Nb_{1.46}O_7$, a = 10.544(1) Å] (all formulas assume $Co^{2.2+}$). The temperature-dependent joins between $CoNb_2O_6$ and the binary Bi–Nb–O phases are consistent with established Bi_2O_3–Nb_2O_5 phase relations. The compound $BiCoO_3$ was not observed under the conditions of this study.

to 93:7 Bi_2O_3:Nb_2O_5. This region has received considerable attention as it forms a series of structurally complex, modulated superstructures[19–23] with variable and potentially useful dielectric properties.[24,25] Reported differences in the detailed phase relations in this region likely arise from kinetic effects, variations in synthesis (especially cooling methods), and/or differences in characterization methods (e.g. X-ray or electron diffraction). For example, the present study, in agreement with early studies,[18] did not find a sillenite-type compound at the composition $Bi_{12}Nb_{0.29}O_{20-x}$.[20] This specimen was a mixture of monoclinic Bi_2O_3 and the fluorite-type solid solution after repeated heatings at 700 °C for a total of 414 h; however, a different heat treatment may have resulted in the metastable body-centered cubic form of Bi_2O_3 (sillenite-type)[26] instead of the monoclinic polymorph.

Ternary phase formation in the Bi_2O_3:$2CoO_{1+x}$:Nb_2O_5 system was found to be limited to pyrochlore, which forms an appreciable solid solution region (Figure 1). During synthesis, the pyrochlore phase formed early in partially reacted samples and was readily purified within the single-phase region, suggesting high thermodynamic stability. Numerous descriptions can be found for the pyrochlore crystal structure, $^{VIII}A_2{}^{VI}B_2O_7$, which is unusual in that it can be considered as two relatively independent interpenetrating networks of [BO_6] octahedra sharing all vertices and [$O'A_4$] tetrahedra in an *anti*-cristobalite-type arrangement.[27–30] The formula is often written as (A_2O')(B_2O_6) or $A_2B_2O_6O'$ to emphasize this interesting structural character and distinguish the two networks. The larger A-cations are eight-fold (= 6+2) coordinated by six oxygen atoms in puckered rings formed by the B_2O_6 network plus two O′ oxygen atoms above and below in the A_2O' network. The structure inherently facilitates non-stoichiometry as the A_2O' network can be partially occupied, or in some cases completely absent; furthermore, numerous non-oxide and halide pyrochlores are known. In addition to extensive compositional ranges, pyrochlores exhibit a remarkable variety of exploitable physical properties, hence the considerable technical importance of this class of solids.[29]

Bi–Co–Nb–O pyrochlores have been previously reported to form at the stoichiometries $Bi_2Co_{2/3}Nb_{4/3}O_7$,[31] $Bi_2Co_3Nb_2O_{12+y}$, $Bi_2Co_4Nb_2O_{13+y}$, and $Bi_2CoNb_2O_{9+y}$;[32] however, under the conditions of the present study none of these compositions are included in the pyrochlore single-phase field: Composition $Bi_2Co_{2/3}Nb_{4/3}O_7$ formed a three-

phase mixture as described in Figure 1; $Bi_2Co_3Nb_2O_{12+y}$ and $Bi_2Co_4Nb_2O_{13+y}$ both occur in three-phase fields consisting of pyrochlore, CoO/Co_3O_4, and a small amount of $CoNb_2O_6$;[33] and the stoichiometry $Bi_2CoNb_2O_{9+y}$ resulted in a three-phase mixture of pyrochlore, $BiNbO_4$, and a small amount of $CoNb_2O_6$. As shown on the diagram (Figure 1), Bi–Co–Nb–O pyrochlores form thermodynamically stable mixtures with the Bi_3NbO_7 solid solution, $Bi_5Nb_3O_{15}$, $BiNbO_4$, $CoNb_2O_6$, $Co_4Nb_2O_9$, and CoO/Co_3O_4. Compositions, nominal formulas, and refined unit cell parameters for single-phase Bi–Co–Nb–O pyrochlores (all dull dark greenish gray in color) prepared in the present study are given in Table 1.[34] The trends in unit cell parameters show a strong dependence on Bi concentration.

Table 1. Compositions, nominal formulas, and unit cell parameters (*a*, space group $Fd\bar{3}m$, #227) for single-phase pyrochlore specimens prepared in this study. These compositions correspond to the points within the five-sided pyrochlore region shown in Figure 1.[34]

Bi_2O_3:$2CoO_{1+x}$:Nb_2O_5	Nominal formula ($Co^{2.2+}$)	*a* [Å]
0.4400:0.2100:0.3500	$Bi_{1.744}Co_{0.8324}Nb_{1.387}O_7$	10.580(1)
0.4200:0.2300:0.3500	$Bi_{1.672}Co_{0.9158}Nb_{1.394}O_7$	10.566(1)
0.4000:0.2200:0.3800	$Bi_{1.562}Co_{0.8594}Nb_{1.484}O_7$	10.556(1)

Observed, indexed X-ray powder diffraction data for the pyrochlore with composition 0.4400:0.2100:0.3500 Bi_2O_3:$2CoO_{1+x}$:Nb_2O_5 are given in Table 2. As noted previously,[29] the 442 reflection, forbidden for an ideal pyrochlore structure, was easily observed in this pattern and in *all* patterns of pyrochlore and pyrochlore-containing specimens prepared in this study. The 442 reflection was also observed in precession photos of single crystals. Similar to the Bi–Zn–Nb–O pyrochlores,[29,35] the observation of this diagnostic reflection indicates the presence of displacements from ideal crystallographic sites. The consistent observation of this reflection indicates that *all* Bi–Co–Nb–O pyrochlores exhibit positional displacements. Furthermore, the stoichiometric location of the pyrochlore phase field, as also found for the analogous Bi–M–Nb–O systems (M = Zn,[29] Fe,[36] Mn[37]), occurs at substantially lower Bi concentrations than conventional formulations placing only Bi on the A sites and the smaller M/Nb cations on the B sites. The pyrochlore field includes compositions with "excess" B cations that require mixing of some Co on the A sites with Bi^{3+}, as found for Zn in *all* Bi–Zn–Nb–O pyrochlores.[29] The limiting compositions observed for the pyrochlore field (Figure 1) suggest that the Co concentration on the A sites can range from ca. 8 to 25%,[38] which is comparable to the analogous ranges observed for other Bi–M–Nb–O pyrochlores with Co replaced by Zn (≈ 16 to 26%),[29] Fe (ca. 4 to 15%),[36] and Mn (ca. 14 to 30%).[37]

Table 2. Observed X-ray powder diffraction data for the pyrochlore with composition Bi_2O_3:$2CoO_{1+x}$:Nb_2O_5 = 0.4400:0.2100:0.3500 [space group $Fd\bar{3}m$, #227, *a* = 10.580(1) Å]. The nominal pyrochlore formula is $Bi_{1.744}Co_{0.8324}Nb_{1.387}O_7$; however, the actual O′ occupancy factor and precise Co oxidation state are uncertain.

h	*k*	*l*	$2\theta_{obsd.}$	$I_{obsd.}$	$2\theta_{calcd.}$	$\Delta 2\theta$	$d_{obsd.}$
1	1	1	14.482	7	14.490	0.007	6.1112
2	2	0	23.757	<1	23.769	0.012	3.7423
3	1	1	27.945	8	27.948	0.003	3.1902
2	2	2	29.217	100	29.218	0.001	3.0541
4	0	0	33.863	35	33.865	0.002	2.6450
3	3	1	37.007	11	37.008	0.001	2.4272
3	3	3	44.460	4	44.461	0.001	2.0361
4	4	0	48.644	50	48.646	0.002	1.8703
5	3	1	51.037	4	51.030	–0.007	1.7881
4	4	2	51.810	1	51.808	–0.003	1.7632
6	2	0	54.854	2	54.838	–0.016	1.6723
5	3	3	57.056	<1	57.038	–0.018	1.6129
6	2	2	57.763	46	57.759	–0.004	1.5948
4	4	4	60.583	13	60.589	0.006	1.5271
7	1	1	62.666	1	62.660	–0.006	1.4813
6	4	2	66.036	<1	66.030	–0.005	1.4136
5	5	3	67.999	<1	68.010	0.011	1.3775

Structural Refinement of the Pyrochlore Phase

The highly symmetrical ideal pyrochlore structure $A_2B_2O_6O'$ crystallizes in space group $Fd\bar{3}m$ with A and B cations on two special positions (16d, 16c) and oxygen atoms on two sites, 48f (O) and 8b (O′), resulting in a single positional variable (*x* for the 48f-site oxygen atoms in the B_2O_6 octahedral network). As expected, this model resulted in anomalously large thermal parameters for the A-site cations and the O′ oxygen atoms in an initial refinement using single-crystal X-ray diffraction data [R_f(obsd.) = 0.325, R_w(obsd.) = 0.237]. The disordered structure was therefore modeled assuming static displacements of the A and O′ atoms, similar to the analogous Bi–M–Nb–O pyrochlores (M = Zn,[35] Fe,[36] Mn[37]) whose structures were refined using neutron powder diffraction data. The Bi:Co:Nb ratio of the single crystal was fixed at a stoichiometry inferred from the refined unit cell parameter of ground crystals [*a* = 10.551(1) Å] taken from the same batch. This value, compared to that for the single-phase pyrochlore powder from which the crystals were grown [*a* = 10.580(1) Å] indicates reduced Bi concentrations in the crystals. When compared to the unit cell parameters obtained for other single-phase pyrochlores (Table 1) and for the limiting compositions of the phase field (cusps, Figure 1), the metal stoichiometry extrapolated for the single crystal was 39.0:24.0:37.0 Bi:Co:Nb. The oxygen content of the crystal was calculated by assuming an average Co oxidation state of 2+, for simplicity, and the O′ sites were assumed to be filled, resulting in an overall formula of $Bi_{1.56}Co_{0.96}Nb_{1.48}O_7$ for the crystals, with fully occupied metal positions.

The refinement of the positional parameters for the disordered metal sites was carried out assuming displacements of the A_2O' network, as found for a number of other pyrochlores.[29,35–37,39–42] Refinement with only Bi displaced gave residuals for observed reflections of R_f = 0.116 and R_w = 0.072 – improved results were obtained when O′ was also displaced. The A site Bi/Co metals were displaced to six partially filled 96g sites; however, the corresponding 96g position for O′ was not stable, and difference Fourier maps consistently showed peaks at and around the ideal 8b site (5/8, 1/8, 1/8). Refinement of the O′ isotropic thermal pa-

Table 3. Refined positional parameters *x*, *y*, *z* and B_{iso} for pyrochlore-type $Bi_{1.56}Co_{0.44}(Co_{0.52}Nb_{1.48})O_7$ at ambient temperature using single-crystal X-ray diffraction data [space group $Fd\bar{3}m$, #227, a = 10.551(1) Å]; R_f(obsd.) = 0.109, R_w(obsd.) = 0.0704.[a]

Atom	Position	*x*	*y*	*z*	B_{iso} [Å^2]	Occ.
Bi/Co	96g	0.5082(15)	0.5082	0.4701(18)	2.66(21)	0.1300/0.0367
Nb/Co	16c	0	0	0	1.46(3)	0.74/0.26
O	48f	1/8	1/8	0.3218(14)	1.8(4)	1.00
O′	32e	0.150(7)	0.150	0.650	4.9(24)	0.25

[a] E.S.D. values. refer to the last digit printed.

rameter diverged, so a displaced position using the 32e site was chosen. Other combinations were not stable. The O′ oxygen position was refined assuming a total contribution of 8 oxygen atoms, hence the occupancy factor of 0.25. The final refinement results are given in Table 3 and illustrated in Figure 2. In the present study, the scattering was dominated by the much heavier Bi and Nb atoms, resulting in limited definition of the displaced oxygen O′ positions. In addition, the disorder on the A and B metal sites hampered a proper refinement of the scale factor due to strong correlations with occupancy parameters. Furthermore, the oxidation state of Co (and therefore oxygen content) and the level of vacancies (if any) on the A and O′ sites were uncertain.[43]

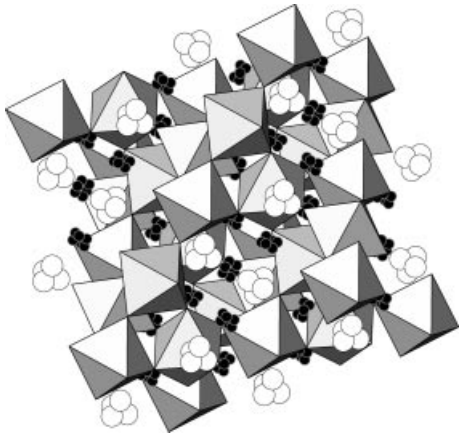

Figure 2. Crystal structure of the pyrochlore $Bi_{1.56}Co_{0.96}Nb_{1.48}O_7$ illustrating the displacive disorder of the A_2O' network (Table 3). The vertex-linked polyhedra represent the octahedral B_2O_6 = $(Co,Nb)_2O_6$ network. The puckered rings of black spheres represent the six equivalent, partially filled 96g sites for the A-site Bi/Co cations; the tetrahedral clusters of larger white spheres denote the four possible positions for O′ oxygens displaced to the 32e sites. The results indicate that the A-site cations are displaced 0.34 Å from the ideal 16d position, while O′ oxygen atoms on 32e sites are displaced 0.45 Å from the high-symmetry 8b position.

The [(Co,Nb)O_6] octahedra in the B_2O_6 network are nearly regular, with metal–oxygen distances of 2.01(1) Å (×6), and O–B–O angles deviating about 3.7° from 90°. The observed bond valence sums calculated about this site[44] using the R_o parameters for Nb^{5+} and Co^{2+} are 4.55 v.u. and 2.52 v.u., respectively. The bonds are therefore longer than expected for Nb–O, suggesting that Co is predominantly present in the 2+ oxidation state, which has a larger sixfold ionic radius (0.745 Å, HS) than Nb^{5+} (0.64 Å) (whereas Co^{3+} is smaller at 0.61 Å, HS).[45] The observed and theoretical bond valence sums for the Nb/Co site using the occupancy factors in Table 3 and assuming the presence of Nb^{5+}/Co^{2+} are 4.03 v.u. and 4.22 v.u., respectively, which are in reasonable agreement given the uncertainties in composition. The A-site Bi/Co metal positions and associated O′ positions are displacively disordered, therefore the A-site coordination sphere is variable. Observed Bi/Co–O distances range from 2.05(5) Å up to 2.96(1) Å. Of these, the distances to the octahedral framework O atoms tend to be longer, ranging from 2.34(1) Å to 2.96(1) Å (with an average of 2.66 Å). The distances between Bi/Co and the displaced O′(32e) atoms are shorter (with an average 2.34 Å) and include the shortest values of 2.05(5) Å, 2.15(5) Å (2x), and 2.25(7) Å (2×), which could reasonably accommodate the smaller Co cations. The equivalent isotropic displacement parameter obtained for the Bi/Co site corresponds to a mean-square displacement of 0.2 Å, as compared with the displacement of 0.34 Å from the ideal site. Similarly, the large displacement parameter for O′ corresponds to a mean-square displacement of 0.25 Å whereas the displacement from the ideal site is 0.45 Å. These values suggest that the large thermal parameters reflect disorder on these sites rather than thermal motion.

The displacive model in Table 3 for the Bi–Co–Nb–O pyrochlore is similar to that reported for a Bi–Fe–Nb–O pyrochlore[36] wherein the A-site cations were displaced 0.43 Å to 96g sites with O′ displaced 0.29 Å to 32e sites. The considerably larger O′ displacement in the Co system (0.45 Å) may reflect the higher concentration of smaller B-type ions on the A sites (≈ 22% compared to <10% in the Fe system). Displacive models for analogous Bi–Zn–Nb–O[35] and Bi–Mn–Nb–O[37] pyrochlores also displaced A sites to 96g sites (0.39 Å and 0.36 Å, respectively), but O′ was displaced differently, to 96g sites (0.46 Å for Zn, 0.33 Å for Mn). Differences in the details of the structural displacements are not unexpected, since the local crystal chemistry and any short-range correlations should be affected by different concentrations of small B-type ions on the A sites as well as variations in the concentrations of vacancies on both the A sites and the O′ sites.

Magnetic Properties of Pyrochlore Phases

Magnetic data obtained for three different single-phase Bi–Co–Nb–O pyrochlore samples indicated qualitatively similar properties. The field dependence of the magnetization confirmed that all samples were overall paramagnetic in nature. The temperature dependence of the magnetic susceptibility, and its inverse, for the pyrochlore with com-

position 0.4000:0.2200:0.3800 Bi_2O_3:$2CoO_{1+x}$:Nb_2O_5 are shown in Figure 3. Above 100 K the inverse magnetic susceptibility was linear and that range was fit to the Curie Weiss law; the results are given in Table 4. For all three compounds, the extrapolation of the linear fits indicated small negative temperature intercepts, suggesting the presence of weak antiferromagnetic cooperative interactions. All of the observed effective magnetic moments calculated from the slopes of the Curie–Weiss fits are higher than the high-spin, spin-only values expected for Co^{2+} ($3d^7$, S = 3/2, 3.87 $\mu\beta$) and Co^{3+} ($3d^6$, S = 2, 4.90 $\mu\beta$), suggesting considerable unquenched orbital contributions, as observed for other Co-containing pyrochlores.[46] Given the range of values previously reported for high-spin Co^{2+} (4.6–5.2 $\mu\beta$/Co) and high-spin Co^{3+} (5.1–5.7 $\mu\beta$/Co)[47] compounds, the observed effective moments for the pyrochlore phases are consistent with the presence of divalent, or mixed divalent-trivalent Co. Slight curvature is observed in the magnetization vs. field data at 10 K (Figure 3, inset). The complex magnetic behavior exhibited by the Bi–Co–Nb–O pyrochlores is

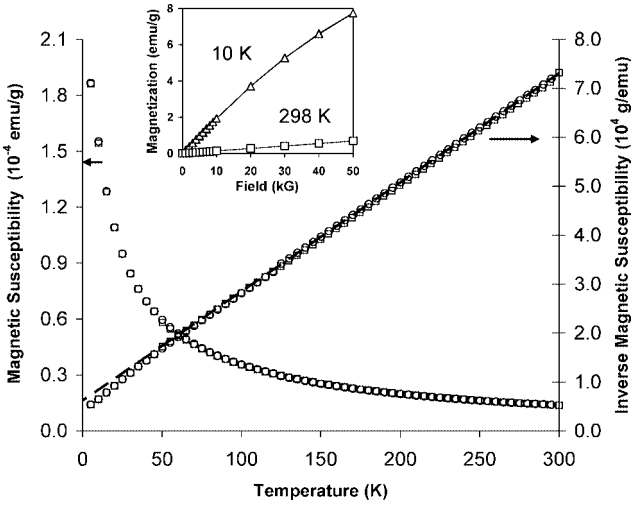

Figure 3. Temperature dependence of the zero-field-cooled (circles) and field-cooled (squares) mass susceptibility and inverse mass susceptibility for the single-phase pyrochlore 0.4000:0.2200:0.3800 Bi_2O_3:$2CoO_{1+x}$:Nb_2O_5 at an applied field of 50 kG. The inset shows the field dependence of the magnetization measured at 10 K (triangles) and 298 K (squares). (Lines are present to guide the eye.) Slight curvature is observed in the low-temperature data. (Units: To convert susceptibility values in emu/g to SI units m^3/kg, multiply by $4\pi/10^3$. To convert field values in Oe (or G) to SI units A/m, multiply by $10^3/4\pi$. Magnetization values in emu/g units are numerically equal to SI units of $A\,m^2$/kg.[48]).

Table 4. Magnetic data for single-phase Bi–Co–Nb–O pyrochlore specimens listed in Table 1. The observed effective moments (μ_{eff}/mol Co) and temperature-axis intercepts (θ, K) were obtained from linear fits of the inverse susceptibility data in the temperature range 100–300 K.

Composition Bi_2O_3:$2CoO_{1+x}$:Nb_2O_5	μ_{eff}/mol Co [$\mu\beta$]	θ [K]
0.4400:0.2100:0.3500	5.1	–35
0.4000:0.2200:0.3800	5.1	–26
0.4200:0.2300:0.3500	5.0	–35

not unexpected given the triangular symmetry of the metal lattices which results in geometric magnetic frustration.[49–50] Pyrochlore compounds are known to exhibit a wide range of cooperative magnetic properties and, for example, are of significant interest as "spin-ice" systems.[51–53]

Dielectric Properties of the Pyrochlore Phase

The relative permittivity (corrected for 10% porosity) and dielectric loss as a function of temperature and frequency for the single-phase pyrochlore with composition 0.4400:0.2100:0.3500 Bi_2O_3:$2CoO_{1+x}$:Nb_2O_5 are shown in Figure 4. The upturns in the data above 250 K indicate that the sample becomes predominantly conductive, and the onset of conductivity is frequency dependent. For example, at 250 K and 1 MHz the sample is still insulating and exhibits a relative permittivity of ca. 115 and tan δ = 0.06, yet at 10 kHz tan δ is greater than 0.2, indicating conductivity. This behavior is in sharp contrast with previously reported bismuth based pyrochlores for which dielectric relaxation is observed.[36,54] The temperature- and frequency-dependent behavior observed is consistent with interfacial polarization mediated by the presence of multivalent Co ions – similar properties were observed for pyrochlores in the Bi–Mn–Nb–O system.[37]

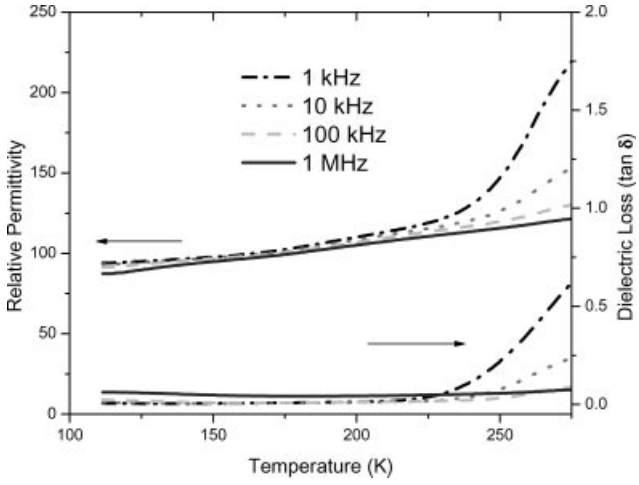

Figure 4. Relative dielectric permittivity (corrected for porosity) and dielectric loss for the single-phase pyrochlore with composition 0.4400:0.2100:0.3500 Bi_2O_3:$2CoO_{1+x}$:Nb_2O_5 at frequencies of 10 kHz, 100 kHz and 1 MHz. The sample is predominantly conductive at temperatures above 250 K and the onset of conductivity is frequency dependent; these effects likely reflect the presence of mixed-valent $Co^{2+/3+}$.

Conclusions

Subsolidus phase relations have been determined for the Bi–Co–Nb–O system in air using specimens equilibrated at 750–925 °C. Ternary phase formation was limited to pyrochlore, which forms a considerable solid solution region at stoichiometries that are "Bi-deficient" compared to conven-

tional $A_2B_2O_7$-type formulations with Bi on the A sites and Co/Nb on the B sites. The location of the pyrochlore field suggests that approximately 8 to 25% of the A sites can be occupied by Co. All Bi–Co–Nb–O pyrochlores form with positional displacements off ideal crystallographic positions, as also found for analogous Bi–M–Nb–O pyrochlores with M = Zn, Fe, and Mn. A structural refinement of the pyrochlore $Bi_{1.56}Co_{0.96}Nb_{1.48}O_7$ using single–crystal X-ray diffraction data is reported with displacements in the A_2O' network. Bi–Co–Nb–O pyrochlores exhibited overall paramagnetic behavior with weak antiferromagnetic interactions; observed effective moments were consistent with the presence of Co^{2+} or $Co^{2+/3+}$ mixtures; however, the observed bond lengths suggest that Co is present predominantly as the larger 2+ ion. Measurements of relative dielectric permittivity and dielectric loss between 110 and 450 K indicated conductive, frequency-dependent properties consistent with the presence of mixed-valent Co. In contrast to $Bi_{1.5}Zn_{0.92}Nb_{1.5}O_{6.92}$, no low-temperature dielectric relaxation was observed. The Bi–Co–Nb–O pyrochlores form thermodynamically stable mixtures with the Bi_3NbO_7 solid solution, $Bi_5Nb_3O_{15}$, $BiNbO_4$, $CoNb_2O_6$, $Co_4Nb_2O_9$, and CoO/Co_3O_4.

Experimental Section

Forty-seven polycrystalline specimens (3–4 g each) were prepared in air by solid-state reactions using Bi_2O_3 (99.999%), Co_3O_4 (99.9985%, pre-analyzed by X-ray powder diffraction), and Nb_2O_5 (99.999%). Prior to each heating, each sample was mixed by grinding with an agate mortar and pestle for 15 min, pelletized, and placed on a bed of sacrificial powder of the same composition supported on alumina ceramic. After an initial calcinations overnight at 800 °C (below the m.p. of Bi_2O_3, 825 °C) multiple 1–3 d heatings (with intermediate grinding and re-pelletizing) were carried out at 875–925 °C.[55] Samples were furnace-cooled to ca. 700 °C and then air-quenched on the bench-top. Metastable melting in non-equilibrated ternary specimens (an initial problem owing to large differences in the melting points of Bi_2O_3, CoO_x, and Nb_2O_5) was avoided by soaking samples at 875 °C for 1–3 d for the second heating, followed by a third heating at 925 °C for 2–3 d. Equilibrium was presumed when no further changes could be detected in the weakest peaks observed in the X-ray powder diffraction patterns. A eutectic in the ternary system may occur near 42:40:18 Bi_2O_3:$2CoO_{1+x}$:Nb_2O_5, which formed liquid at 900 °C. Bi_2O_3 volatilization was observed above the solidus by thermogravimetric analysis, but was not detectable in the subsolidus study. Pyrochlore-type crystals were easily obtained by heating a single-phase polycrystalline specimen (composition 0.4400:0.2100:0.3500 Bi_2O_3:$2CoO_{1+x}$:Nb_2O_5) in a Pt capsule (sealed by welding) to 1300 °C, followed by slow cooling (4 °C/h) to below the freezing point (≈1160 °C). The crystals exhibited conchoidal fracture and were obtained as brown-black shards.

Phase assemblages were ascertained using the disappearing phase method[56,57] and X-ray powder diffraction data obtained with a Philips[58] diffractometer equipped with incident Soller slits, a theta-compensating slit and graphite monochromator, and a scintillation detector. Samples were mounted in welled glass slides. Patterns were collected at ambient temperatures using Cu-K_α radiation over the range 3–70° 2θ with a 0.02° 2θ step size and a 2 s count time. Intensity data measured as relative peak heights above background were obtained using the DATASCAN software package, and processed using JADE. For unit cell refinements, observed 2θ line positions were first corrected using SRM 660, LaB_6,[59] as an external calibrant. Lattice parameters were refined using JADE (2θ values, Cu-$K_{\alpha1}$ = 1.540593 Å).

Preliminary characterization of pyrochlore-type single crystals was carried out using the precession camera method (Zr-filtered Mo-K_α radiation) to assess quality, cell parameter, and space group. Data for structural refinement were collected with an Oxford Diffraction Xcalibur 2 CCD diffractometer with graphite-monochromated Mo-K_α radiation. Due to the strong absorption coefficient of 50.2 mm^{-1}, several small crystals with approximate dimensions 0.03 mm × 0.04 mm × 0.04 mm were chosen, and measurements included 2θ angles up to 100°. However, large absorption corrections were still required and limited the range of observable reflections. Further details of the crystal-structure investigation may be obtained from the Fachinformationzentrum Karlsruhe, 76344 Eggenstein-Leopoldshafen, Germany, on quoting the depository number CSD-416601.

Magnetic properties were characterized with a Quantum Design SQUID magnetometer and single-phase polycrystalline samples. Magnetization was measured as a function of temperature between 2 K and 300 K after cooling in the absence of an applied field (zero-field cooled, ZFC) and while cooling in a magnetic field (field-cooled, FC) of 50 kG between 2 K and 300 K. In addition, measurements at 10 K and at 298 K were carried out to determine the field dependence of the magnetization in applied fields between 0 and 50 kG.

Dielectric properties were evaluated using pellets prepared from single-phase powders mixed with 2 wt.-% PVA (polyvinyl alcohol) to assist forming. Mixtures were ground using a mortar and pestle, sieved (300 μm mesh), and then dried at 120 °C for 5 min. Approximately 0.6 g of the mixture was uniaxially pressed into a disk (ca. 1 mm thick, ca. 10 mm diameter) using a pressure of ca. 180 MPa. The green pellets were then sintered in air at 975 °C for 4 h. The density of the sintered samples was measured in water using Archimedes's principle and compared to the theoretical density of the material. Gold/palladium electrodes (ca. 75 nm thick) were sputtered onto the top and bottom surfaces to form parallel plate capacitors. The complex dielectric permittivity was measured between 1 kHz and 1 MHz using an Agilent 4284 LCR meter. The sample temperature was controlled with a programmable 9023 Delta Design for measurements between 110 and 450 K.

Acknowledgments

We thank L. P. Cook for thermogravimetric analyses, N. Swanson for graphical representation of the phase diagram data, and R. Drew and R. D. Shull for assistance with magnetic measurements. M. C. Y. was supported in part by the National Science Foundation's Research Experience for Undergraduates (REU) program, Division of Materials Research.

[1] N. A. Spaldin, M. Fiebig, *Science* **2005**, *309*, 391–392.
[2] V. E. Wood, A. E. Austin, in: *Magnetoelectric Interaction Phenomena in Crystals* (Eds.: A. J. Freeman, H. Schmid), Gordon and Breach, London, **1975**.
[3] N. A. Hill, *J. Phys. Chem. B* **2000**, *104*, 6694–6709, and references therein.
[4] P. Baettig, N. A. Spaldin, *Appl. Phys. Lett.* **2005**, *86*, 012505 (article number), and references therein.

[5] D. V. Efremov, J. Van Den Brink, D. I. Khomskii, *Nat. Mater.* **2004**, *3*, 853–856.
[6] N. A. Spaldin, W. E. Pickett, *J. Solid State Chem.* **2003**, *176*, 615–632.
[7] C. Ederer, N. A. Spaldin, *Phys. Rev. B* **2005**, *71*, 060401 (article number) and references cited therein.
[8] T. Kimura, S. Kawamoto, I. Yamada, M. Azuma, M. Takano, Y. Tokura, *Phys. Rev. B* **2003**, *67*, 180401 (article number), and references therein.
[9] B. B. Van Aken, T. T. M. Palstra, A. Filippetti, N. A. Spaldin, *Nature* **2004**, *3*, 164–170, and references therein.
[10] M. Kenzelmann, A. B. Harris, S. Jonas, C. Broholm, J. Schefer, S. B. Kim, C. L. Zhang, S. W. Cheong, O. P. Vajk, J. W. Lynn, *Phys. Rev. Lett.* **2005**, *95*, 087206 (article number), and references therein.
[11] O. P. Vajk, M. Kenzelmann, J. W. Lynn, S. B. Kim, S. W. Cheong, *Phys. Rev. Lett.* **2005**, *94*, 087601 (article number), and references therein.
[12] M. Azuma, K. Takata, T. Saito, S. Ishiwata, Y. Shimakawa, M. Takano, *J. Am. Chem. Soc.* **2005**, *127*, 8889–8892.
[13] *Phase Equilibria Diagrams* (formerly Phase Diagrams for Ceramists), The American Ceramic Society, Westerville, Ohio; Figs, 6:6391, EC-096.
[14] A. Burdese, M. Lucco-Borlera, P. Rolando, *Atti Accad. Sci. Torino, Cl. Sci. Fis., Mater. Nat.* **1964**, *99*, 565–575.
[15] A. Ramanan, J. Gopalakrishnan, *Indian J. Chem. Sect. A* **1985**, *24*, 594.
[16] N. Rangavittal, T. N. Guru Row, C. N. R. Rao, *Eur. J. Solid State Inorg. Chem.* **1994**, *31*, 409.
[17] Y. Uratani, T. Shishidou, F. Ishii, T. Oguchi, *Japn. J. Appl. Phys.* **2005**, *44*, 7130–7133.
[18] R. S. Roth, J. L. Waring, *J. Res. Natl. Bur. Stand.* **1962**, *66A*, 451.
[19] R. L. Withers, C. D. Ling, S. Schmid, *Z. Kristallogr.* **1999**, *214*, 296–304.
[20] C. D. Ling, R. L. Withers, S. Schmid, J. G. Thompson, *J. Solid State Chem.* **1998**, *137*, 42.
[21] M. Valant, B. Jancar, U. Pirnat, D. Suvorov, *J. Eur. Ceram. Soc.* **2005**, *25*, 2829–2834.
[22] U. Pirnat, M. Valant, B. Jancar, D. Suvorov, *Chem. Mater.* **2005**, *17*, 5155–5160.
[23] C. D. Ling, M. Johnson, *J. Solid State Chem.* **2004**, *177*, 1838–1846.
[24] M. Valant, D. Suvorov, *J. Am. Ceram. Soc.* **2003**, *86*, 939.
[25] M. Valant, D. Suvorov, *J. Am. Ceram. Soc.* **2004**, *87*, 1056–1061.
[26] E. M. Levin, R. S. Roth, *J. Res. Natl. Bur. Stand.* **1964**, *68A*, 189–195.
[27] A. F. Wells, *Structural Inorganic Chemistry*, Clarendon Press, Oxford, 4th edition, **1975**, p. 499.
[28] M. A. Subramanian, G. Aravamudan, G. V. S. Rao, *Prog. Solid State Chem.* **1983**, *15*, 55.
[29] T. A. Vanderah, I. Levin, M. W. Lufaso, *Eur. J. Inorg. Chem.* **2005**, *14*, 2895–2901, and references therein.
[30] R. L. Withers, W. Somophon, V. P. Ting, Y. Liu, Q. Zhou, B. J. Kennedy, *J. Solid State Chem.*, in press (**2006**).
[31] G. A. Smolenskii, V. A. Isupov, G. I. Golovshchifova, A. G. Tutov, *Inorg. Mater.* **1976**, *12*, 255–258.
[32] I. V. Piir, D. A. Prikhodko, S. V. Ignatchenko, A. V. Schukariov, *Solid State Ionics* **1997**, *101–103*, 1141–1146.
[33] More accurately, these points occur within the four-phase compatibility volume (Bi_2O_3–CoO–Co_3O_4–$CoNb_2O_6$). The relations in the four-component system actually studied here (Bi_2O_3–CoO–Co_3O_4–Nb_2O_5) have been projected onto a ternary slice (Figure 1) to simplify presentation of the results.
[34] Although the metal ratios given here are precise, the actual populations on the A and B sites depend on the O′ occupancy factor and Co oxidation state(s), which are uncertain and which may vary in each pyrochlore. Expressions for the structural formulas for the pyrochlore phases are therefore ambiguous. For purposes of comparison, the formulas have been normalized to seven oxygens (full occupancy of the O′ site) and assume an average oxidation state of 2.2+ for Co; the reasons for the latter assumption are described in the text.
[35] I. Levin, T. G. Amos, J. C. Nino, T. A. Vanderah, C. A. Randall, M. T. Lanagan, *J. Solid State Chem.* **2002**, *168*, 69.
[36] M. W. Lufaso, T. A. Vanderah, I. M. Pazos, I. Levin, J. C. Nino, V. Provenzano, P. K. Schenck, submitted to *J. Solid State Chem.*.
[37] T. A. Vanderah, M. W. Lufaso, A. U. Adler, I. Levin, J. C. Nino, V. Provenzano, P. K. Schenck, *J. Solid State Chem.*, in press.
[38] Estimated by assuming a range of average Co oxidation states from 2.0+ to 2.5+, and full occupancy of the O' site; the latter assumption results in maximum estimates for $Co_{A\ site}$ concentrations and minimum estimates for A-site vacancy concentrations.
[39] M. Ganne, K. Toyama, *Mater. Res. Bull.* **1975**, *10*, 1313.
[40] M. Avdeev, M. K. Haas, J. D. Jorgensen, R. J. Cava, *J. Solid State Chem.* **2002**, *169*, 24.
[41] L. Q. Li, B. J. Kennedy, *Chem. Mater.* **2003**, *15*, 4060.
[42] Ismunandar, T. Kamiyama, K. Oikawa, A. Hoshikawa, B. J. Kennedy, Y. Kubota, K. Kato, *Mater. Res. Bull.* **2004**, *39*, 553.
[43] These results should be considered as an approximation of the disordered structure; the large differences in X-ray scattering factors suggests that neutron diffraction techniques may yield a more detailed picture of the structural disorder.
[44] N. E. Brese, M. O'Keeffe, *Acta Crystallogr., Sect. B* **1991**, *47*, 192–197, with updated R_o parameters http://www.ccp14.ac.uk/ccp/web-mirrors/i_d_brown/.
[45] R. D. Shannon, *Acta Crystallogr., Sect. A* **1976**, *32*, 751.
[46] M. K. Haas, R. J. Cava, M. Avdeev, J. J. Jorgensen, *Phys. Rev. B* **2002**, *66*, 094429.
[47] R. L. Carlin, Magnetochemistry, Springer-Verlag, Berlin, **1986**, chapter 4.
[48] R. B. Goldfarb, *Concise Encyclopedia of Superconducting and Magnetic Materials* (Ed.: J. Evetts), Pergamon Press, Oxford, **1992**, p. 256..
[49] J. E. Greedan, *J. Mater. Chem.* **2001**, *11*, 37.
[50] K. Ramesha, L. Sebastian, B. Eichhorn, J. Gopalakrishnan, *J. Mater. Chem.* **2003**, *13*, 2011.
[51] A. P. Ramirez, A. Hayashi, R. J. Cava, R. Siddharthan, B. S. Shastry, *Nature* **1999**, *399*, 333.
[52] R. Siddharthan, B. S. Shastry, A. P. Ramirez, A. Hayashi, R. J. Cava, S. Rosenkranz, *Phys. Rev. Lett.* **1999**, *83*, 1854.
[53] G. D. Blundred, C. A. Bridges, M. J. Rosseinsky, *Angew. Chem. Int. Ed.* **2004**, *43*, 3562.
[54] J. C. Nino, H. J. Youn, M. T. Lanagan, C. A. Randall, *J. Mater. Res.* **2002**, *17*, 1178.
[55] Exceptions: specimens with Bi contents at least 70 mol-% were not heated above 750 °C (to avoid melting and decomposition of sillenite-type phases), and those with Bi contents less than 30 mol-% were heated at higher final temperatures, 950–1300 °C, to achieve equilibrium more quickly.
[56] C. G. Bergeron, S. H. Risbud, *Introduction to Phase Equilibria in Ceramics*, American Ceramic Society, Westerville, **1984**.
[57] C. S. Barrett, *Structure of Metals*, McGraw-Hill, New York, **1943**, chapter X, 1st edition.
[58] Certain commercial equipment and software are identified in order to adequately specify the experimental procedure; recommendation or endorsement by the National Institute of Standards and Technology is not therein implied.
[59] C. R. Hubbard, Y. Zhang, R. L. McKenzie, *Certificate of Analysis, SRM 660*, National Institute of Standards and Technology, Gaithersburg, MD, 20899, **1989**.

Received: July 13, 2006
Published Online: October 5, 2006

